Innovation in rangeland monitoring: annual, 30 m, plant functional type percent cover maps for U.S. rangelands, 1984–2017

Matthew O. Jones [ID],[1,2],† Brady W. Allred,[1,2] David E. Naugle,[2] Jeremy D. Maestas,[3]
Patrick Donnelly [ID],[4] Loretta J. Metz,[5] Jason Karl,[6] Rob Smith,[7] Brandon Bestelmeyer,[8] Chad Boyd,[9]
Jay D. Kerby,[10] and James D. McIver[11]

[1]Numerical Terradynamic Simulation Group, University of Montana, 32 Campus Drive, Missoula, Montana 59812 USA
[2]W.A. Franke College of Forestry and Conservation, University of Montana, 32 Campus Drive, Missoula, Montana 59812 USA
[3]Natural Resources Conservation Service, West National Technology Support Center, Portland, Oregon 97232 USA
[4]Intermountain West Joint Venture, United States Fish and Wildlife Service, 32 Campus Drive, Forestry Building 302, Missoula, Montana 59812 USA
[5]Resource Assessment Division, USDA-Natural Resources Conservation Service, Temple, Texas 76502 USA
[6]Department of Forest, Rangeland, and Fire Sciences, University of Idaho, Moscow, Idaho 83844 USA
[7]Department of Computer Science, College of Humanities and Sciences, University of Montana, 32 Campus Drive, Missoula, Montana 59812 USA
[8]Jornada Experimental Range, USDA Agricultural Research Service, P.O. Box 30003, MSC 3JER, NMSU, Las Cruces, New Mexico 88003 USA
[9]Eastern Oregon Agricultural Research Center, USDA Agricultural Research Service, 67826-A Hwy. 205, Burns, Oregon 97720 USA
[10]The Nature Conservancy, 67826-A Hwy. 205, Burns, Oregon 97720 USA
[11]Eastern Oregon Agriculture Research Center, Oregon State University, 372 S 10th Street, Union, Oregon 97883 USA

Abstract. Innovations in machine learning and cloud-based computing were merged with historical remote sensing and field data to provide the first moderate resolution, annual, percent cover maps of plant functional types across rangeland ecosystems to effectively and efficiently respond to pressing challenges facing conservation of biodiversity and ecosystem services. We utilized the historical Landsat satellite record, gridded meteorology, abiotic land surface data, and over 30,000 field plots within a Random Forests model to predict per-pixel percent cover of annual forbs and grasses, perennial forbs and grasses, shrubs, and bare ground over the western United States from 1984 to 2017. Results were validated using three independent collections of plot-level measurements, and resulting maps display land cover variation in response to changes in climate, disturbance, and management. The maps, which will be updated annually at the end of each year, provide exciting opportunities to expand and improve rangeland conservation, monitoring, and management. The data open new doors for scientific investigation at an unprecedented blend of temporal fidelity, spatial resolution, and geographic scale.

† **E-mail:** matt.jones@ntsg.umt.edu

INTRODUCTION

Efficient data collection and landscape monitoring in space and time are critical for responding to global challenges impacting preservation of biodiversity. Integration of new technology with existing large-scale, long-term data collection efforts can improve our understanding of ecosystem threats leading to more effective conservation strategies (Marvin et al. 2016). Satellite remote sensing platforms offer over four decades of temporal records documenting ecological and land use dynamics of Earth's biomes. Land cover maps derived from these data have proven invaluable to informing conservation but have been limited by computational tradeoffs that constrain their temporal or spatial resolution. Integration of new cloud-based computing and image archive platforms (Gorelick et al. 2017) into traditional land cover mapping may now transcend shortfalls to advance conservation solutions (Snaddon et al. 2013) by filling long-standing information gaps in dynamic ecosystem monitoring (Hansen et al. 2013, Donchyts et al. 2016).

At large scales, land cover mapping adheres to tradeoffs that must balance spatial and temporal resolution and categorical vs. continuous delineations (i.e., each pixel as a single land cover type vs. percent cover of multiple land cover types). Global products that supply categorical land cover (Arino et al. 2008) can provide high temporal resolution data (Friedl et al. 2010) capable of tracking ecosystem dynamics but do so at coarse spatial resolution (>300 m). These data provide important insight into landscape-level change but do not translate directly to finer ecosystem interactions. In contrast, moderate resolution (30 m) categorical maps at continental (Ryan and Opperman 2013, Homer et al. 2015) or global extents (Chen et al. 2015) and regional continuous maps (Xian et al. 2013, 2015) provide higher-order information, but behave as snapshots in time due to five- or ten-year lags between evaluations. Missing is land cover monitoring that combines the virtues of high spatial and temporal resolution needed to inform local ecological outcomes that are inherently dynamic and difficult to predict.

Land cover field protocols record the presence, frequency, or relative coverage of species, plant functional types (PFT), or abiotic components (e.g., bare soil, rock) in recognition that, at nearly any scale, the majority of the natural land surface is heterogeneous. Categorical maps are simplifications of this complex heterogeneous land surface, creating unrealistic ecotone boundaries and limiting our ability to accurately model and monitor ecological processes at resolutions relevant to inform or monitor land management and assess conservation efforts. For example, primary productivity models (Running and Zhao 2015, Robinson et al. 2018) require parameters that represent vegetation attributes and functional characteristics, and use of categorical maps results in a single set of parameters over a pixel that may contain numerous PFT with significant functional variation. Categorical delineations also confound species distribution and habitat models when species display preferences for heterogeneous landscapes or PFT cover thresholds (Lipsey and Naugle 2017), especially if the minimal presence of a specific PFT (e.g., tree species encroachment into shrub communities) equates to habitat loss (Miller et al. 2017). Mapping the migration or establishment of PFTs and the spread or susceptibility of an area to invasive species is also lacking as categorical classes represent the dominant cover type. The presence of an invasive species may not be mapped until it dominates an area, preventing timely initiation of management activities to prevent or mitigate spread. Continuous estimates of cover remove these limitations as they preserve the heterogeneity of field measures and provide assessments of vegetation composition, density, and biomass variability, all of which are key indicators of ecosystem biodiversity, function, resilience, and resistance (Allen and Hoekstra 1991, Ostfeld et al. 1997).

The innovation presented in this manuscript is the use of emerging technologies (Gorelick et al. 2017) and machine learning (Breiman 2001) to map continuous estimates of land cover which required processing vast amounts of data that were logistically prohibitive before. Remote sensing has proven an adequate and low-cost solution for land cover monitoring that provides continuous coverage at multiple spatiotemporal scales (Booth and Tueller 2003, Hunt et al. 2003, Sant et al. 2014, Xian et al. 2015, McCord et al. 2017), but challenges have remained as the

geographic area and time period of interest increased data volume and computational processing, both becoming significant barriers to implementation. The increased availability and use of high-performance cloud computing, storage, and services removes such barriers. Combining these technologies with traditional plot-level monitoring programs permits the creation of land cover datasets with complete geographic and temporal coverage.

In the United States, rangelands are estimated to cover approximately 2.6–3.0 million square kilometers (Havstad et al. 2009, Reeves and Mitchell 2011), nearly one-third of the total U.S. land area, providing vital ecosystem services, including water, mineral and wood resources, livestock grazing, wildlife habitat, recreation, and cultural heritage. Population growth and increased demand for the goods and services that rangelands provide, have affected the spatial extent and degree of rangeland fragmentation (Havstad et al. 2009). This demand has manifest land cover changes in the form of cultivation for crops (Smith et al. 2016), energy development (Allred et al. 2015), and altered fire regimes (Miller et al. 2013). These changes, coupled with drought, climate effects (Huang et al. 2017), and changes in species composition (particularly from non-native invasive plants or encroachment of native woody plants), are affecting rangeland resilience and resistance with cascading effects on ecosystem services (Brooks et al. 2016, Maestas et al. 2016, Chambers et al. 2017).

Mapping continuous rangeland cover at temporal and spatial scales relevant to on-the-ground conservation would provide needed clarity for reducing threats and informing adaptive management in a rapidly changing world. To this end, we implement Google Earth Engine, a cloud computing platform for planetary-scale analysis (Gorelick et al. 2017), the Random Forests (RF; Breiman 2001) machine learning algorithm, and traditional large-scale field sampling efforts to produce annual (1984–2017), moderate resolution (30 m), percent land cover maps of four classes: annual forbs and grasses (AFG), perennial forbs and grasses (PFG), shrubs (SHR), and bare ground (BG), for rangelands across the western United States with the capability to produce annual updates at the end of each year. In this manuscript, we (1) detail the methods and

land cover models which capitalize on these emerging technologies, (2) display the resulting land cover maps, (3) provide error and validation metrics for each of the land cover classes, and (4) demonstrate the utility of these maps for rangeland management, assessment, and monitoring at broad scales.

METHODS

Spatial and temporal extents

The spatial extent and resulting maps cover all rangelands of the western United States from the Pacific Coast to the eastern border of Great Plains states (Fig. 1). The bounds are based on the spatial extent and density of plot-level measures used to train and validate the land cover models. For visualizations, non-rangelands are masked using a coterminous U.S. Rangelands 30 m circa 2011 product (Reeves and Mitchell 2011). Land cover maps are produced annually from 1984 to 2017 with the temporal bounds defined by the historic period of the Landsat surface reflectance (SR) data product, inclusive of the Landsat 5 TM, Landsat 7 ETM+, and Landsat 8 OLI sensors.

Vegetation field plots

We used the Natural Resources Conservation Service (NRCS) National Resources Inventory (NRI; USDA NRCS 2015), the Bureau of Land Management (BLM) Assessment, Inventory, and Monitoring (AIM) Landscape Monitoring Framework (LMF), and BLM TerrADat datasets (hereafter referred to as NRI-AIM field plots) across western U.S. rangelands (Fig. 1) to train and validate land cover models. The combination of these field plots provided 31,130 plots collected with a standardized protocol from 2004 to 2016 across non-federal and public BLM lands. Data collection methods for NRI and AIM (LMF and TerrADat) field plots are described in Herrick et al. (2017) and MacKinnon et al. (2011), respectively. Both methods use the same line-point-intercept protocol where two 150-foot transects, oriented northeast to southwest and northwest to southeast, are centered on the sample point. A pin is dropped at 3-foot intervals along each transect recording the presence of plants by species, litter, rock fragment, and bare ground. In this application, we use the first hit pin drop data to calculate cover (a method to best represent cover
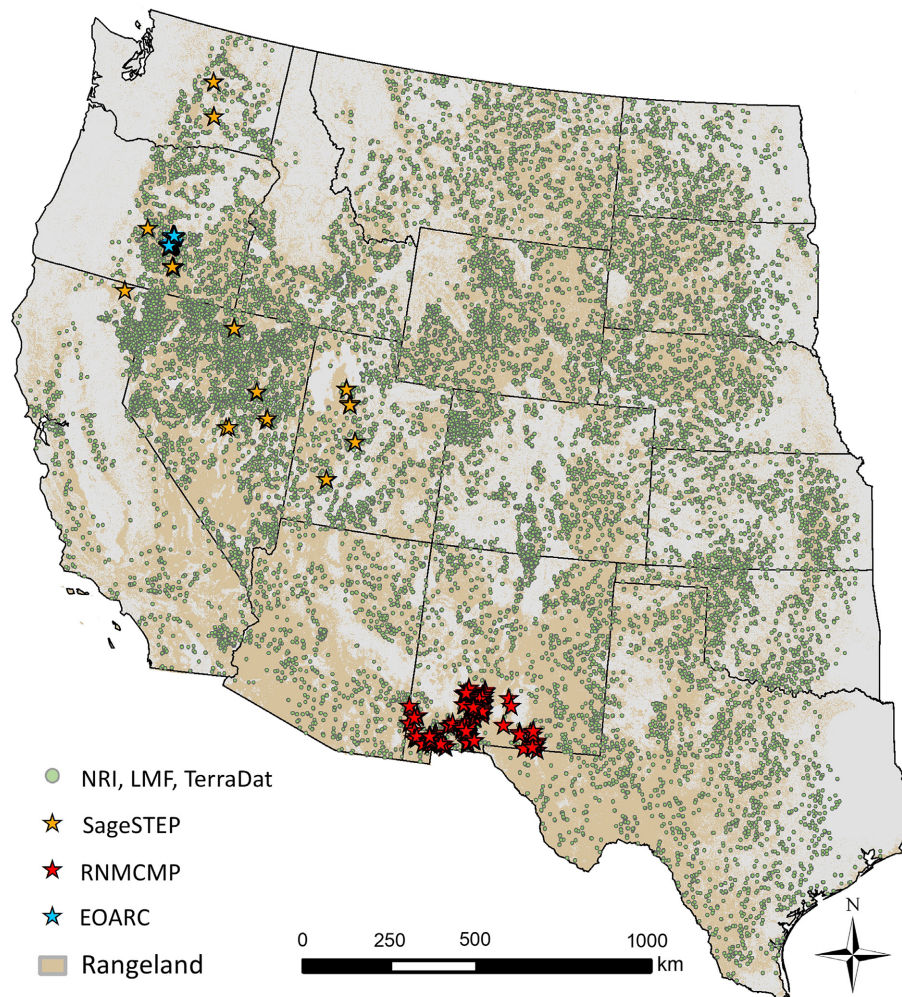
Fig. 1. Extent of study area. Points are Natural Resources Conservation Service National Resources Inventory (NRI) and Bureau of Land Management Assessment, Inventory, and Monitoring Landscape Monitoring Framework (LMF) and TerraADat plots used for training and validating the Random Forests model. Stars show locations of independent plot-level measures of cover from the Sagebrush Steppe Treatment Evaluation Project (SageSTEP), the Restore New Mexico Collaborative Monitoring Program (RNMCMP) initiative, and the Eastern Oregon Agricultural Research Center (EOARC) used to validate model results.

from a remote sensing perspective) and species-level data are aggregated into three functional groups: AFG, PFG, and SHR based on definitions in the USDA NRCS PLANTS database (USDA NRCS 2018), and the bare ground (BG) measure is retained resulting in percent cover estimates per plot for four classes: AFG, PFG, SHR, and BG.

Landsat satellite data

The Landsat 5 TM, 7 ETM+, and 8 OLI SR Collection products (30 m) are the highest level of

processing available for Landsat imagery and are calibrated across sensors and corrected for atmospheric effects and illumination/viewing geometry (Masek et al. 2006, Vermote et al. 2016). The 30 m resolution of the Landsat data is used as the minimum mapping unit for the resulting land cover maps. Capitalizing on the computational capability of Google Earth Engine (EE; Gorelick et al. 2017), we analyzed all Landsat TM, ETM+, and OLI scenes over the study region from 1984 to 2017, 231,053 Landsat scenes in

total. The Landsat data were masked for cloud-contaminated, cloud shadow, and saturated SR retrievals to calculate pixelwise seasonal SR metrics, a suite of vegetation and moisture indices, and tasseled-cap (TC) transformations (Table 1). For each year, seasonal SR means (spring, April–June; summer, July–September; fall, October–December) were calculated using all unmasked pixels; winter (January–March) SR retrievals were not included due to excessive snow and cloud cover. Vegetation indices (USGS EROS 2017) and TC transformations (Baig et al. 2014) were calculated for every unmasked retrieval, and then, seasonal means, minimums, and maximums were derived, as well as differences in seasonal maximums (Table 1). The Landsat data (as

well as the meteorological and abiotic data described below) were reprojected and bilinearly interpolated to a geographic coordinate system (WGS-84; EPSG:4326) at ~30 m resolution after calculating seasonal and annual metrics.

Meteorological data

The University of Idaho Gridded Surface Meteorological Dataset (GRIDMET) provides daily surface meteorological fields from 1979 to the present at ~4 km resolution across the continental U.S. (Abatzoglou 2013). We used daily fields of temperature, precipitation, and potential evapotranspiration to derive seasonal and annual metrics (Table 1). For each year (1984–2017), total and seasonal precipitation, total

Table 1. Spatial temporally dynamic and static (see *Notes*) variables used to train Random Forests land cover models and predict land cover.

Spatial temporally dynamic variables	Seasonal‡	Seasonal differences	Annual
Landsat surface reflectance bands†			
Blue (Band 2, 480 nm)	$\bar{x}_i, \bar{x}_j, \bar{x}_k$		
Green (Band 3, 560 nm)	$\bar{x}_i, \bar{x}_j, \bar{x}_k$		
Red (Band 4, 655 nm)	$\bar{x}_i, \bar{x}_j, \bar{x}_k$		
NIR (Band 5, 865 nm)	$\bar{x}_i, \bar{x}_j, \bar{x}_k$		
SWIR 1 (Band 6, 1161 nm)	$\bar{x}_i, \bar{x}_j, \bar{x}_k$		
SWIR 2 (Band 7, 2200 nm)	$\bar{x}_i, \bar{x}_j, \bar{x}_k$		
Vegetation indices§			
NDVI (normalized difference vegetation index)	$(\bar{x}, x_{\min}, x_{\max})_{i,j,k}$	$\bar{x}_i - \bar{x}_j, \bar{x}_j - \bar{x}_k$	
EVI (enhanced vegetation index)	$(\bar{x}, x_{\min}, x_{\max})_{i,j,k}$	$\bar{x}_i - \bar{x}_j, \bar{x}_j - \bar{x}_k$	
SAVI (soil adjusted vegetation index)	$(\bar{x}, x_{\min}, x_{\max})_{i,j,k}$	$\bar{x}_i - \bar{x}_j, \bar{x}_j - \bar{x}_k$	
MSAVI (modified soil adjusted vegetation index)	$(\bar{x}, x_{\min}, x_{\max})_{i,j,k}$	$\bar{x}_i - \bar{x}_j, \bar{x}_j - \bar{x}_k$	
NDMI (normalized difference moisture index)	$(\bar{x}, x_{\min}, x_{\max})_{i,j,k}$	$\bar{x}_i - \bar{x}_j, \bar{x}_j - \bar{x}_k$	
NBR (normalized burn ratio)	$(\bar{x}, x_{\min}, x_{\max})_{i,j,k}$	$\bar{x}_i - \bar{x}_j, \bar{x}_j - \bar{x}_k$	
NBR2 (normalized burn ratio 2)	$(\bar{x}, x_{\min}, x_{\max})_{i,j,k}$	$\bar{x}_i - \bar{x}_j, \bar{x}_j - \bar{x}_k$	
Tasseled-cap transformations			
TC green	$(\bar{x}, x_{\min}, x_{\max})_{i,j,k}$	$\bar{x}_i - \bar{x}_j, \bar{x}_j - \bar{x}_k$	
TC brightness	$(\bar{x}, x_{\min}, x_{\max})_{i,j,k}$	$\bar{x}_i - \bar{x}_j, \bar{x}_j - \bar{x}_k$	
TC water	$(\bar{x}, x_{\min}, x_{\max})_{i,j,k}$	$\bar{x}_i - \bar{x}_j, \bar{x}_j - \bar{x}_k$	
TC 4	$(\bar{x}, x_{\min}, x_{\max})_{i,j,k}$	$\bar{x}_i - \bar{x}_j, \bar{x}_j - \bar{x}_k$	
TC 5	$(\bar{x}, x_{\min}, x_{\max})_{i,j,k}$	$\bar{x}_i - \bar{x}_j, \bar{x}_j - \bar{x}_k$	
TC 6	$(\bar{x}, x_{\min}, x_{\max})_{i,j,k}$	$\bar{x}_i - \bar{x}_j, \bar{x}_j - \bar{x}_k$	
Meteorological data¶			
Precipitation (p)	$\sum_i, \sum_j, \sum_k, \sum_l$	$\sum_i - \sum_j, \sum_j - \sum_k$	$\sum$
Minimum and maximum temperature			P10, P50, P90
Potential evapotranspiration (pet)			$\sum$
Water deficit			$\sum_p - \sum_{\mathrm{pet}}$

Notes: All layers were reprojected and bilinearly interpolated to a geographic coordinate system (WGS-84) at approximately 30 m resolution. Temporally static variables. gSSURGO Soils: %sand, %silt, %clay, pH, available water (0–25 cm), elect. conductivity, organic matter. Topography: elevation, slope, heat index, height above nearest drainage. Location: pixel latitude, pixel longitude.
† Landsat 8 OLI band numbers and band centers shown for reference.
‡ Seasons i, j, k, l as Spring (April–June), Summer (July–September), Fall (October–December), Winter (January–March).
§ Landsat Surface Reflectance-Derived Spectral Indices (USGS EROS 2017).
¶ Meteorological statistics calculated for current year and previous year. P is percentiles.

evapotranspiration, and the 10th, 50th, and 90th percentiles of minimum and maximum temperatures were calculated. We also derived second-order metrics, including an estimate of annual water deficit (total precipitation minus total potential evapotranspiration) and seasonal precipitation differences (spring minus summer precipitation; summer minus fall precipitation).

Abiotic land surface data

A suite of gridded, temporally static 30-m abiotic land surface data products were also incorporated (Table 1). From the USGS National Elevation Dataset, we produced layers of elevation and slope and used a gridded dataset defining Height Above Nearest Drainage (Rennó et al. 2008, Nobre et al. 2011). Pixel center coordinates of latitude and longitude were included as model variables, and using slope, aspect, latitude, and longitude, we produced a heat index following the methods of McCune and Keon (2002). Using the FY2016 Gridded Soil Survey Geographic (gSSURGO) Database (the most detailed level of soil geographic data developed by the National Cooperative Soil Survey), we mapped a set of 30-m-resolution soil attributes across the study region: percent sand, silt, and clay, organic matter, available water capacity from 0 to 25 cm, pH, and electrical conductivity (Soil Survey Staff 2017).

Sampling spatiotemporal data

Landsat, meteorological, and abiotic data together provided 215 gridded 30 m variables (Table 1) for predicting land cover percentages. The selection of the 215 variables was based on well-established scientific investigations and literature that demonstrate PFT variation in cover is related to climate, meteorological patterns (both seasonal and annual), topography, and soil conditions and that remotely sensed measures of SR, vegetation and moisture indices, and TC transformations (and seasonal magnitudes and differences therein) vary based on the type and extent of vegetation and bare ground cover. Using EE, the static abiotic and spatiotemporal land surface values were extracted over each NRI-AIM field plot using the single pixel nearest to the plot center location (i.e., a nearest neighbor approach). The spatiotemporal data were sampled for the year corresponding to the year the

field plot was measured, including the previous year's meteorological data which have been shown to influence current-year vegetation cover (Pilliod et al. 2017*a*). The sampling provided a table of 215 spatiotemporal and static variables including the percent cover values for 27,643 NRI-AIM field plots for use in RF regression models. Plots with missing data for any variable (e.g., excessive cloud cover, SR saturation) were excluded.

Random Forests

Random Forests (Breiman 2001) is a non-parametric machine learning method that utilizes an ensemble of regression trees, has been shown to have higher classification accuracy than simple regression methods (Belgiu and Drăguţ 2016, Gómez et al. 2016), is robust to overfitting (each regression tree retains an independent fraction of the data [0.368] for validation, known as out-of-bag [OOB] samples) and has grown in prominence for mapping land cover with a multitude of small-scale and regional studies and applications (Riley et al. 2016, Azzari and Lobell 2017, West et al. 2017, Anderson et al. 2018). Random Forests has the ability to model complex non-linear interactions across predictors, leveraging the large quantity of high spatial resolution plot cover estimates with the vast suite of spatiotemporal and static predictor variables.

Land cover model training and prediction

We used the R (R Core Team, 2017) ranger package (Wright and Ziegler 2017) to define RF model parameters and select the optimal input variables, and then implemented RF in EE to predict percent cover values across the study region. The ranger package provides diagnostic tools and variable importance ranking which are not available in the EE RF method. First, RF was implemented individually for each land cover class (AFG, PFG, SHR, BG) using the table of 27,643 NRI-AIM field plots and all 215 variables. Variables were ranked by importance using an impurity measure (the variance of the responses; Louppe et al. 2013) resulting in ranks of variable importance specific to each land cover. Random Forests was then iteratively implemented for each land cover class using the highest ranked variable and adding the next highest ranked variable at each subsequent run. Root mean square

errors of the OOB field plots for each iteration were used to determine the number of variables at which errors were minimized for each land cover class (Genuer et al. 2010, Chen and Ishwaran 2012).

Error curves varied for each class with asymptotes occurring at a range of approximately 5–40 variables (Fig. 2). Although a class-specific number of variables could be used for each model, we used the top 40 variables per class (Appendix S1: Table S1) in land cover predictions. The justification for using 40 variables was to balance error minimization with computation efficiency, to maintain a consistent model structure of 40 variables across classes, that errors did not increase with the addition of variables beyond the asymptote (e.g. SHR, AFG), and to not limit the predictive power of the model in future runs as field plots are added. For example, as additional plots are included for model training and prediction, it cannot be assumed that error minimization will occur at the same fixed minimum number of variables for each class.

The table of sampled NRI-AIM field plots (27,643) was then used to train RF models in EE using the optimized RF parameters from the
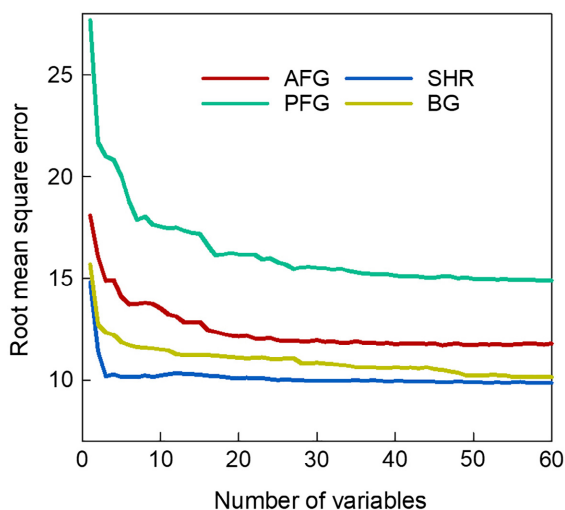

Fig. 2. Random Forests model (used within the R ranger package) root mean square error for first 60 of 100 model iterations; the next most important variable is added at each iteration. Model runs are conducted independently for each class (AFG, annual forbs and grasses; BG, bare ground; PFG, perennial forbs and grasses; SHR, shrubs).

ranger implementation. After model training, 30-m gridded data cubes of the 40 highest ranking variables for each land cover class and year were assembled in EE which were then used as model input to predict pixelwise annual percent cover at 30 m resolution from 1984 to 2017. The model prediction step alone required the processing and co-registering of a minimum of 1360 geospatial layers, or over 4.7 TB of data—demonstrating the power of cloud computing and EE.

Validation of continuous land cover

Percent land cover predictions were validated using error estimates of OOB samples (NRI-AIM field plots withheld from model training) in the ranger and EE implementations of RF. Although RF in ranger and EE implement the same published methods (Breiman 2001), we calculated root mean square errors (RMSE) and mean absolute error (MAE) between OOB percent land cover predictions and field plot measures for both ranger and EE models to ensure that errors were similar. The OOB error estimation provides the mean prediction error for every NRI-AIM field plot, using only predictions from the RF regression trees that did not have that field plot in the subset of data used for training. To estimate confidence intervals we examined the variability of OOB predictions (Wager et al. 2014), a method available within the ranger RF package (detailed methods in Appendix S1).

We also validated the continuous land cover maps using three independent collections of field data (Table 2, Fig. 1) from the Sagebrush Steppe Treatment Evaluation Project (McIver et al. 2010, SageSTEP; a collaborative Great Basin effort to evaluate sagebrush restoration), the Restore New Mexico Collaborative Monitoring Program initiative (BLM and USDA-ARS Jornada Experimental Range collaborative effort to evaluate restoration treatments), and a collaborative project from the USDA Agricultural Research Service and The Nature Conservancy collocated at the Eastern Oregon Agricultural Research Center (EOARC). We aggregated project data to percent cover per plot for the AFG, PFG, SHR, and BG land cover classes (BG measurements were only available for SageSTEP). We calculated differences between plot measurements and the average predicted land cover values (AFG, PFG, SHR, BG) for all pixels that intersected the plot boundaries.

Table 2. Projects that provided field plots of percent cover values used for validation.

Project	Years	Plots	N	Description
Sagebrush Steppe Treatment Evaluation Project (SageSTEP)	2006–2014	52	253	Plots contained 15–24 subplots (30 × 33 m); 852 subplots total. Five line transects measured in each subplot. Subplot cover aggregated to plot-level cover for validation
Restore New Mexico Collaborative Monitoring Program	2007–2017	183	868	Plots consist of paired parallel 50-m transects 20 m apart. Percent cover for each transect used for validation
Eastern Oregon Agricultural Research Center	2016	198	198	Plots (30 × 30 m) contained three 20-m transects. Plot-level percent cover used for validation

Note: N is total number of plot-level measures used for validation.

RESULTS

Land cover maps

Annual percent cover maps from 1984 to 2017 at 30 m resolution for the four land cover classes were produced across the full study region. Maps of year 2016 for the four classes (AFG, PFG, SHR, BG) are displayed in Fig. 3 with non-rangeland systems masked. Maps of vegetation cover are also combined (Fig. 4) where the vegetation classes are represented using a red (AFG), green (PFG), blue (SHR) color palette providing a visual representation of land cover heterogeneity (BG not shown) for year 2016 across the study region; a heterogeneous pixel displays the resulting blend of colors along a gradient that scales according to the per-pixel percent cover of each class. Online visualization and analysis of the land cover maps is available via the Rangeland Analysis Platform (https://rangelands.app).

Validation and error metrics

Validation summary statistics of MAE and RMSE from the OOB samples (NRI-AIM field plots) for ranger and EE implementations of RF are provided in Table 3, with RMSEs of 11.8%, 14.9%, 9.9%, and 10.6% for AFG, PFG, SHR, and BG (respectively) for the EE RF model used for land cover predictions across the study region. Examination of errors between the ranger and EE RF model implementations showed minimal disparity with no error difference greater than 0.5% between the two implementations. The errors are equivalent or lower than RMSEs from similar efforts to map continuous rangeland cover, where McCord et al. (2017) used a Bayesian additive regression tree and reported RMSEs ranging from 11% to 14% for BG, herbaceous, and shrub classes, and Xian et al. (2013) used regression tree modeling and reported errors ranging from 9.7% to 14.4% for AFG, SHR, and BG classes.

Estimations of prediction confidence using variance of OOB predictions (Wager et al. 2014) demonstrated that errors scaled somewhat with increasing field plot cover values for AFG, SHR, and BG, but remained constant for PFG (Appendix S1: Fig. S1), with all classes displaying RMSEs across field plot cover values relatively equivalent to the summarized RMSEs in Table 3. The increase in error with field plot cover for AFG, SHR, and BG can be partially attributed to the skewed distribution of cover values in the NRI/AIM field plots. Only 7%, 2%, and 9% of the field plots had measured cover values over 50% for AFG, SHR, and BG, respectively, resulting in minimal samples with high cover values used in model training.

Fig. 5 displays scatter plots of NRI-AIM field plot measures vs. OOB predictions and least-squares linear regressions results for each land cover class from the ranger RF model (AFG: $r^2 = 0.49$, $P < 0.001$, standard error of the estimate (SEE) = 7.74; PFG: $r^2 = 0.75$, $P < 0.001$, SEE = 12.45; SHR: $r^2 = 0.43$, $P < 0.001$, SEE = 6.14; BG: $r^2 = 0.71$, $P < 0.001$, SEE = 8.22). Errors between OOB percent land cover predictions and NRI-AIM field plot measures are also presented spatially (Appendix S1: Fig. S2) providing a geographic visual of error distribution.

For the three independent collections of field data, validation summary statistics of MAE and RMSE between percent land cover predictions and plot-level measures are also provided in Table 3. Root mean square errors ranged from 7.1% to 17.7% across land cover classes and projects. Fig. 5 displays scatter plots of the independent collections of field data vs. land cover predictions and least-squares linear regressions results for each land cover class (AFG: $r^2 = 0.19$,
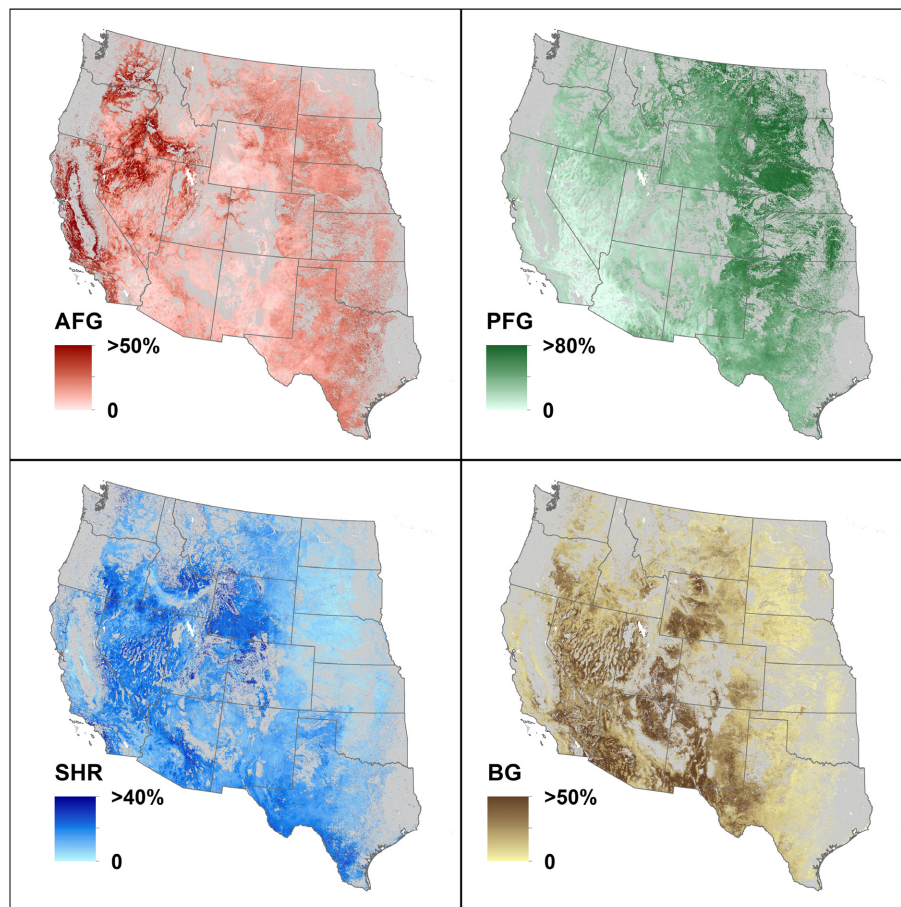
Fig. 3. Continuous land cover maps of annual forbs and grasses (AFG), perennial forbs and grasses (PFG), shrubs (SHR), and bare ground (BG) for year 2016. Gray and white areas are non-rangeland pixels based on a coterminous U.S. Rangelands 30 m circa 2011 product (Reeves and Mitchell 2011) and water, respectively.

$P < 0.001$, SEE = 4.61; PFG: $r^2 = 0.16$, $P < 0.001$, SEE = 6.03; SHR: $r^2 = 0.04$, $P < 0.001$, SEE = 5.18; BG: $r^2 = 0.49$, $P < 0.001$, SEE = 5.32).

The scatter plots and regressions (Fig. 5) show that the model performed better when predicting OOB validation plots vs. the independent field plots. This may be attributable to the variation in plot protocols, size, and orientation across the three projects (Table 2), none of which followed the same protocols as the NRI-AIM field plots used to train the model.

DISCUSSION

For the first time, we produced annual, historical (1984–2017) percent land cover maps by PFT for western U.S. rangelands. Utilizing spatiotemporal robust ground-level measurements, contiguous long-term land surface and climate variables, and large-scale data processing and modeling capability, we estimated percent cover of AFG, PFG, shrubs, and bare ground at approximately 30 m resolution. These datasets better capture the spatiotemporal variability of land cover than commonly used categorical datasets and build upon other continuous datasets that are limited in geographic and temporal extent, resolution, and PFT. Overcoming these limitations allows for examination of land cover dynamics that are particularly important for the long-term monitoring, conservation, assessment, and management of U.S. rangelands.

With continuous rather than categorical estimates of vegetation cover, it is possible to assess
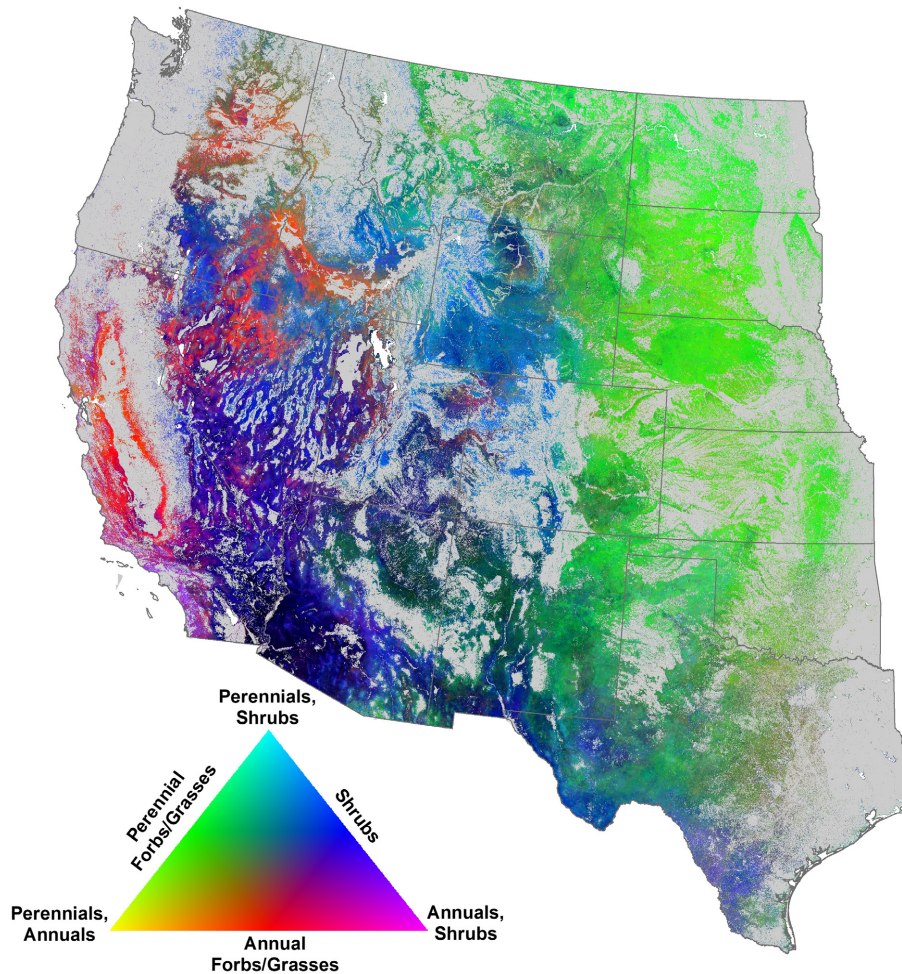
Fig. 4. A color gradient map of three vegetation classes; annual forbs and grasses, perennial forbs and grasses, and shrubs mapped to red, green, and blue (respectively, as shown in Fig. 3 maps) displaying the heterogeneity and dominance of vegetation cover classes per pixel for year 2016. Gray and white areas are non-rangeland and water, respectively. Bare ground class not included in visualization.

changes in functional group composition, transitions to new vegetation states, efficacy of vegetation treatments, and vegetation dynamics pre- and post-disturbance across space and time. Evaluations can be summarized at broad scales (e.g., landscapes, watersheds, allotments, or pastures) while also permitting examination of the variation within such boundaries. The ability to examine spatial variation allows energy, management activities, and financial resources to be focused on locations that need the most attention. Temporal trends enable the examination of vegetation dynamics through time, which is especially useful in areas where historical data or

knowledge is lacking. Such information can be particularly helpful in restoration after a disturbance (e.g., wildfire), where knowledge of rangeland condition pre-disturbance is critical to designing effective restoration (Miller et al. 2013). We provide two examples demonstrating the benefits of continuous cover estimates and their utility for rangeland monitoring and management.

Wildfire and treatments

Catastrophic wildfire is a critical threat in one of North America's largest terrestrial ecosystems, the sagebrush steppe (Miller et al. 2013). Pre-fire vegetation composition is known to heavily

Table 3. Mean absolute error (MAE) and root mean square error from ranger and Earth Engine (EE) Random Forests out-of-bag (OOB) error estimates, and percent cover between model results and independent plot-level measures from three projects: the Sagebrush Steppe Treatment Evaluation Project (SageSTEP), the Restore New Mexico Collaborative Monitoring Program (RNMCMP) initiative, and a project from the Eastern Oregon Agricultural Research Center (EOARC).

Land Cover	OOB ranger	OOB EE	SageSTEP	RNMCMP	EOARC
Annual Forbs/grasses	8.1|12.0	7.8|11.8	8.2|11.5	7.5|14.8	7.3|10.0
Perennial Forbs/grasses	11.6|15.2	11.2|14.9	13.2|17.7	11.0|14.9	10.8|13.2
Shrubs	7.2|10.1	6.9|9.9	9.2|11.0	5.6|7.1	8.1|10.6
Bare ground	7.0|10.1	7.3|10.6	9.4|12.5		

Notes: Error values displayed as MAE|RMSE. Bare ground percent cover values available for SageSTEP only.
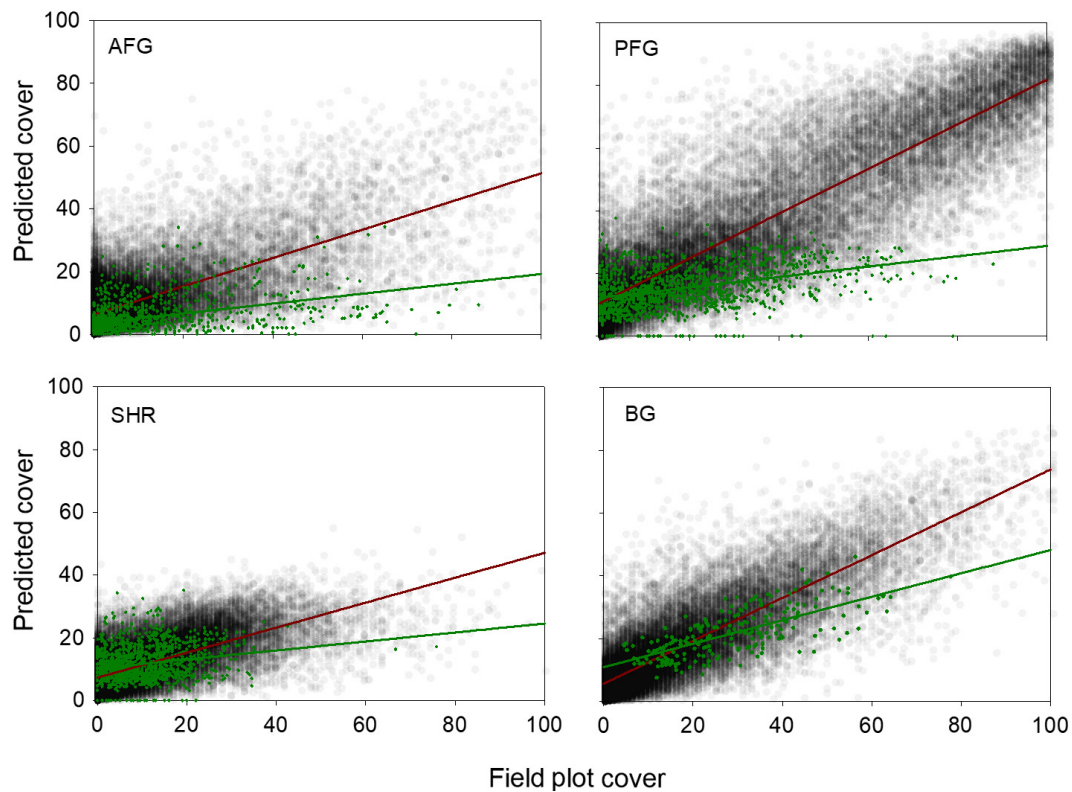

Fig. 5. Scatter plots of National Resources Inventory-Assessment, Inventory, and Monitoring field plot percent cover of annual forbs and grasses (AFG), perennial forbs and grasses (PFG), shrubs (SHR), and bare ground (BG) vs. Random Forests out-of-bag predicted percent cover (gray points) and linear least-squares regression results (red line); AFG: $r^2 = 0.49$, $P < 0.001$, standard error of the estimate (SEE) = 7.74; PFG: $r^2 = 0.75$, $P < 0.001$, SEE = 12.45; SHR: $r^2 = 0.43$, $P < 0.001$, SEE = 6.14; BG: $r^2 = 0.71$, $P < 0.001$, SEE = 8.22. Overlaid are scatter plots of field plot percent cover from independent field plots vs. predicted percent cover (green points) and linear least-squares regression results (green line); AFG: $r^2 = 0.19$, $P < 0.001$, SEE = 4.61; PFG: $r^2 = 0.16$, $P < 0.001$, SEE = 6.03; SHR: $r^2 = 0.04$, $P < 0.001$, SEE = 5.18; BG: $r^2 = 0.49$, $P < 0.001$, SEE = 5.32. BG for independent field plots was available from only a single project.

influence post-fire succession, along with fire severity, weather, soils, and other abiotic factors (Miller et al. 2013). Typically, areas dominated by native PFG are more resilient to fire and are more likely to return to sagebrush rangelands over time. Areas with low native perennial forb and grass cover and an invasive annual forb or grass presence may be dominated by annuals post-fire and undergo undesired ecological state shifts (Chambers et al. 2014), with subsequent impacts to ecosystem resilience, wildlife habitat, and rural economies (Miller et al. 2011). Therefore, land managers often plan post-fire treatments to reduce invasive annual plant abundance and seed desired perennials to mitigate risks, but uncertainty about pre-fire conditions over such large landscapes hinders the ability to triage areas in most need of intervention. Integrating our historical continuous land cover estimates with local data and knowledge and available geospatial layers of burn severity (e.g., MTBS), weather (e.g., GRIDMET), and abiotic indicators of potential resilience and resistance (Miller et al. 2013, Maestas et al. 2016) can help managers more effectively and efficiently target limited resources.

We illustrate the utility of our new monitoring capability using the lightning-caused 2015 Soda Fire which burned nearly 280,000 acres of sagebrush rangeland along the southern border of Idaho and Oregon (Fig. 6). Immediately post-fire, an Emergency Stabilization and Burned Area Rehabilitation plan was implemented to stabilize and restore burned areas, increase perennial grasses and shrubs, and reduce invasive annual species at a cost of more than $60 million (BLM 2015). Treatments included seeding and seedling plantings, and aerial herbicide application to suppress invasive annual grasses. Summarizing land cover pre- and post-fire within the Soda Fire perimeter reveals expected trends for western sagebrush ecosystems: Annual herbaceous vegetation and bare ground increased the year after the fire, while perennial herbaceous vegetation and fire-intolerant shrubs decreased. Spatial examination also shows that increases and decreases were not consistent across the fire but varied greatly (Fig. 6).

The new monitoring tool presented here also provides knowledge of historical pre-fire vegetation cover which can inform restoration plans and resource allocation where more local data or

knowledge is absent and enables evaluation of treatment impact and vegetation state changes through time. Aerial herbicide applications (Pilliod and Welty 2013, Pilliod et al. 2017b, designed to reduce invasive annuals) applied immediately post-fire in the fall 2015 and one year later (2016) show decreases in AFG in the years following treatment with abrupt contrasts in AFG cover values along treatment boundaries (Fig. 7). It is important to note that we are not evaluating the efficacy of these treatments; such an evaluation is out of the scope of this paper and is better conducted by those with more detailed information concerning treatment application, surface conditions, and application timing, etc., and would require thorough analysis of model error in relation to the magnitude of estimated change (Table 3; Appendix S1: Fig. S1). The historical land cover dynamics also enable analysis of effects of previous disturbance within the same region, in this case a 2002 fire that burned within the Soda Fire perimeter (Fig. 7). Examining the annual herbaceous dynamics of a single treatment within the Soda Fire shows that in the 1980s, annual herbaceous cover ranged from approximately 8–20% (Fig. 7). Cover of annuals began to increase in the early 2000s and peaked just before the 2002 wildfire. Subsequently, it appears a vegetation state shift ensued, with altered perennial cover dynamics and reduced shrub cover, accompanied by a dominance of annuals. Annual herbaceous cover exhibited extreme fluctuations following the 2002 fire, peaking the year following the Soda Fire and prior to herbicide application.

Grazing and rangeland health

Evaluating rangeland health and the effects of livestock grazing has long been a core objective of rangeland monitoring and adaptive management across private and public lands (West 2003). Ground cover and composition metrics are commonly included in assessments of whether or not land health standards are being achieved (Pellant et al. 2005) with most inventory and monitoring following traditional sampling protocols (e.g., line-point-intercept plots) at individual site scales. Transect-based estimates provide important fine-resolution data but can be difficult to extrapolate to conditions at broader pasture or allotment scales where management decisions are often made. Combining these
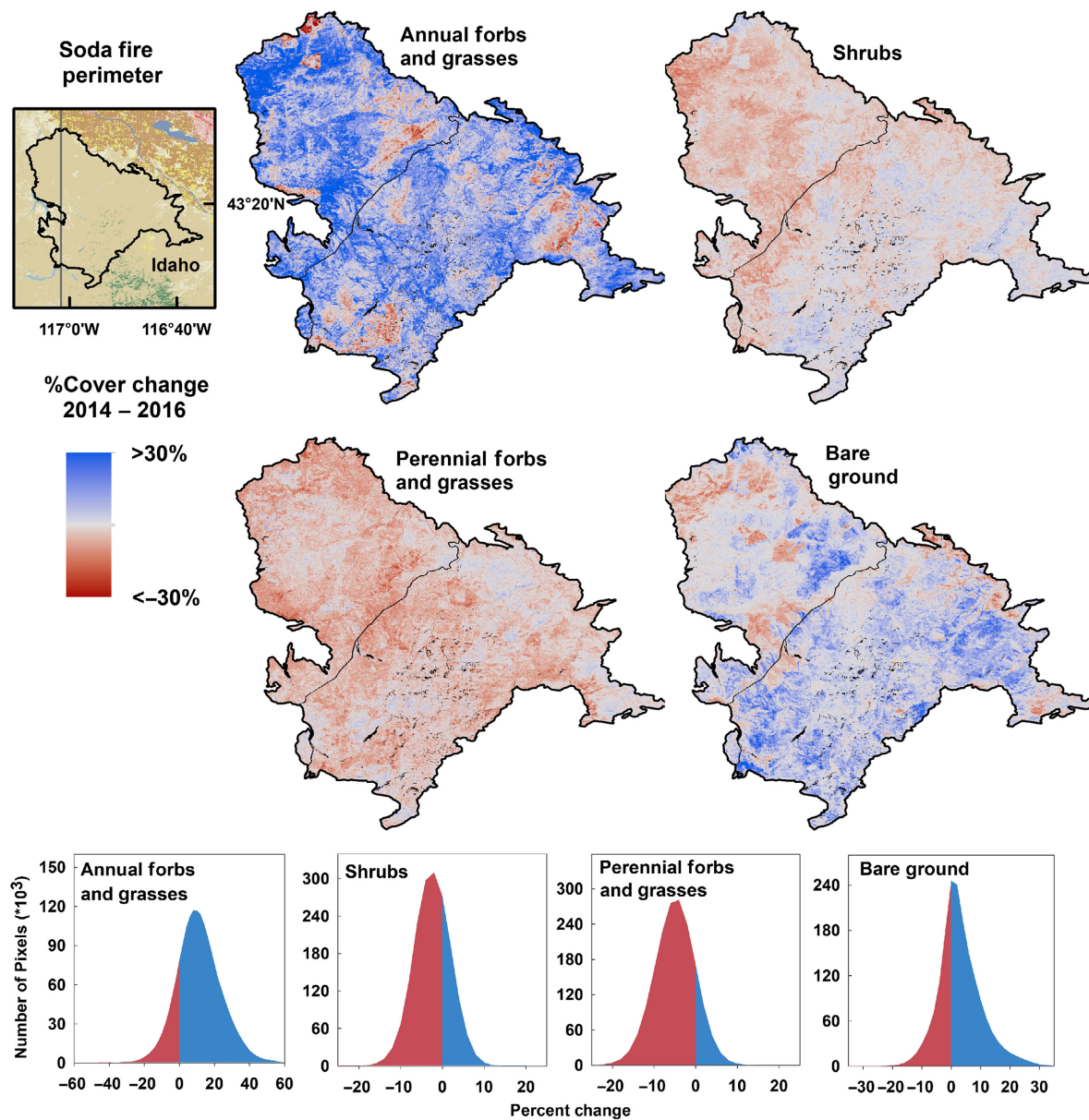
Fig. 6. Location of Soda Fire (2015) and maps of estimated change in percent cover from pre- (2014) to post-fire (2016) for four classes within the Soda Fire perimeter (top). Histograms of percent change for each class (bottom).

traditional approaches with our continuous land cover maps provides new temporal and landscape perspective for local observations.

To illustrate, we provide a historical record of land cover estimates over a 6000-ha grazing allotment administered by the BLM in Montana, USA. Annual means of AFG, PFG, SHR, and BG cover and total precipitation within the allotment are shown alongside photographs detailing the same point of view from years 2002 and 2010 (provided by the BLM Billings, Montana Field Office; Fig. 8). Land managers can use this information to consider how site-level conditions relate to overall conditions in the surrounding area and assess whether changes in functional groups are within the normal range of variability or perhaps responding to management, weather, and climate, or other factors. Of course, detailed
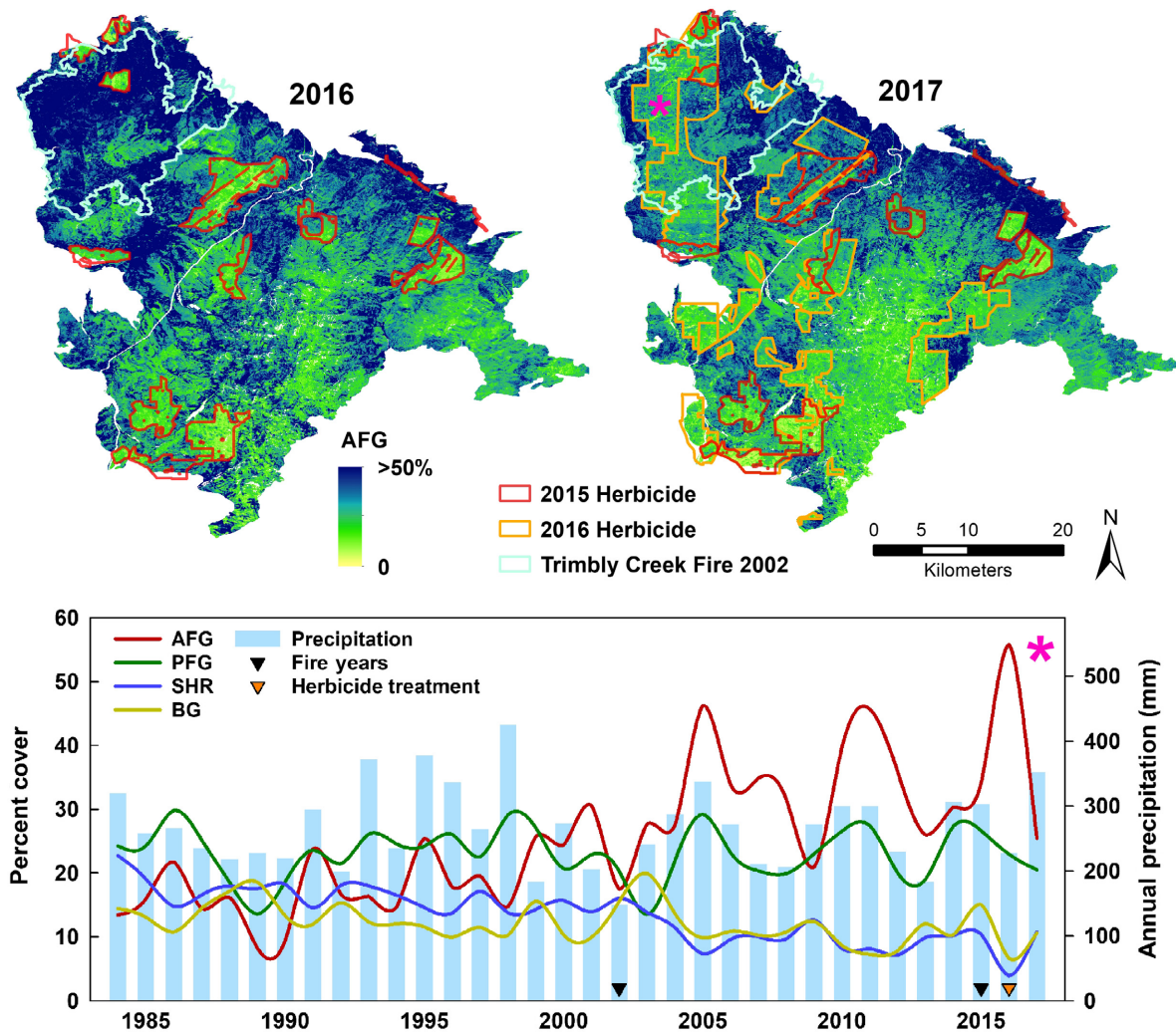
Fig. 7. Percent cover of annual forbs and grasses (AFG) for years 2016 and 2017 within the Soda Fire (2015) perimeter. Polygons display herbicide treatments to reduce invasive annuals applied post-fire in fall of 2015 (red) and 2016 (orange), and boundary of Trimbly Creek Fire (2002). Time series of a single 2016 treatment polygon (pink star) displays average percent land cover for AFG, perennial forbs and grasses (PFG), shrubs (SHR), and bare ground (BG), including annual precipitation, fire years, and herbicide treatment year. Only herbicide treatments are shown and may not be a complete record of treatments. Multiple other historic and post-fire treatments (seeding, planting, etc.) are not included.

knowledge of the site history, grazing strategies, and more, along with consideration of model error in relation to change (Table 3; Appendix S1: Fig. S1), is needed to make informed adaptive management decisions. We simply demonstrate the value-added information provided by historical maps produced at a temporal and spatial scale that permits evaluations both within and across allotments.

Conclusion

The ability to examine historical to present trends of land cover across broad geographies at 30 m spatial resolution provides exciting opportunities to expand and improve rangeland conservation and management. These annually updated cover maps will facilitate ongoing evaluation of conservation programs, management
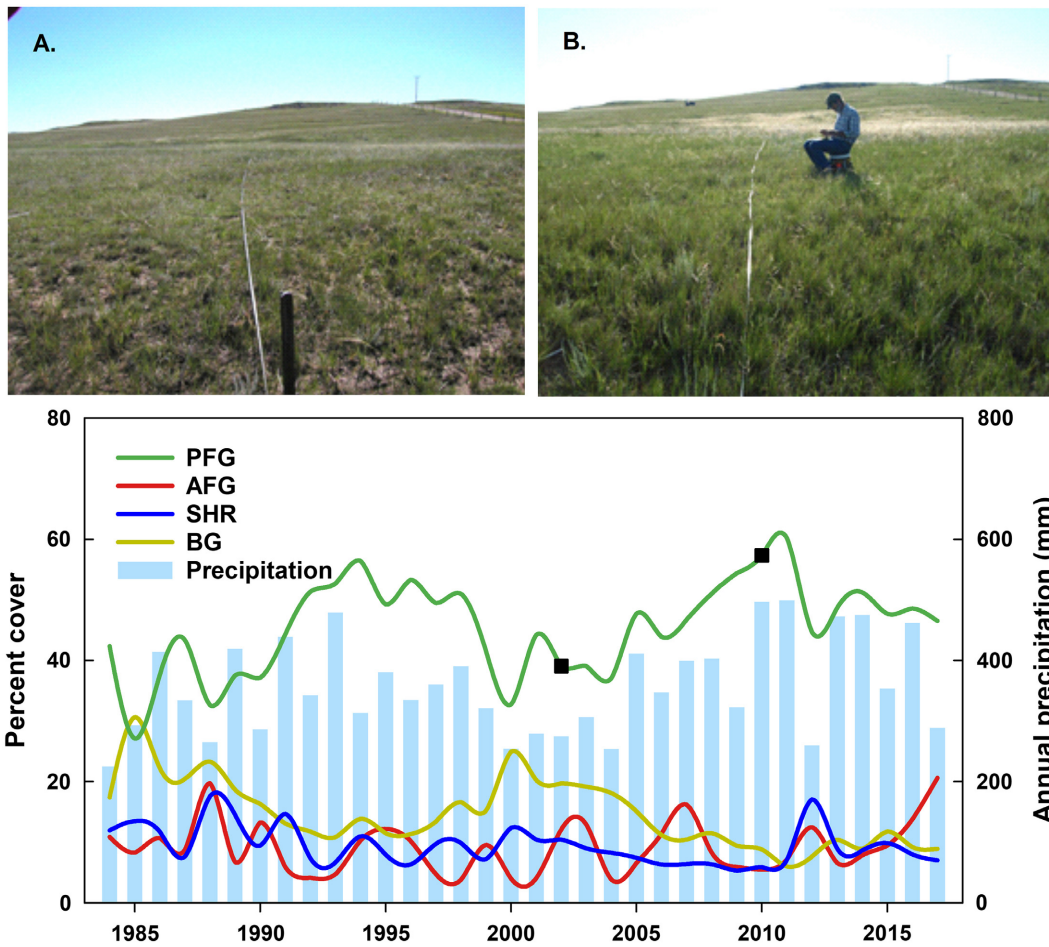
Fig. 8. Photographs of a Bureau of Land Management grazing allotment in Montana, USA, taken from the same point of view in years 2002 (A) and 2010 (B). Plot displays annual precipitation and percent cover means within the allotment for four land cover classes, perennial forbs and grasses (PFG), annual forbs and grasses (AFG), shrubs (SHR), and bare ground (BG) from 1984 to 2017. Black squares are years of photographs.

changes, and overall rangeland conditions. Private or public rangeland managers can use cover maps to evaluate previous management actions, but more importantly to guide future management decisions. Coupled with intimate, local knowledge of their system, managers can use these tools to gain a historical perspective and to plan specifically for their objectives. The integration of PFT maps into agency (i.e., BLM, NRCS, and USFS) specific programs and future strategies enhances broad-scale evaluation of rangeland core indicators (McCord et al. 2017). Our work highlights the importance of large-scale systematic monitoring programs like the NRCS NRI and BLM AIM, which provided essential field plot data in the creation of these cover maps; future support for additional field plot data will increase samples and likely improve overall model accuracy and prediction.

The maps presented here are the result of a synergistic coupling of moderate resolution long-term remote sensing products, vast collections of historical field data, advanced machine learning algorithms, and cloud-based computing. This coupling provides an advancement in land cover mapping where the resulting maps begin to match the inherent heterogeneity of the landscape and can be produced annually at minimal time-lags (within months of year's end). This advancement opens new doors for monitoring, conservation,

and scientific investigation at an unprecedented blend of temporal fidelity, spatial resolution, and geographic scale. The future of such maps can only improve as new remote sensing data, the continuation of field campaigns, cloud computing platforms, and advanced machine learning algorithms become available and accessible.

ACKNOWLEDGMENTS

LITERATURE CITED

Abatzoglou, J. T. 2013. Development of gridded surface meteorological data for ecological applications and modelling. International Journal of Climatology 33:121–131.

Allen, T. F. H., and T. W. Hoekstra. 1991. Role of heterogeneity in scaling of ecological systems under analysis. Pages 47–68 in J. Kolasa and S. T. A. Pickett, editors. Ecological heterogeneity. Springer, New York, New York, USA.

Allred, B. W., W. K. Smith, D. Twidwell, J. H. Haggerty, S. W. Running, D. E. Naugle, and S. D. Fuhlendorf. 2015. Sustainability. Ecosystem services lost to oil and gas in North America. Science 348:401–402.

Anderson, K. E., N. F. Glenn, L. P. Spaete, D. J. Shinneman, D. S. Pilliod, R. S. Arkle, S. K. McIlroy, and D. R. Derryberry. 2018. Estimating vegetation biomass and cover across large plots in shrub and grass dominated drylands using terrestrial lidar and machine learning. Ecological Indicators 84:793–802.

Arino, O., P. Bicheron, F. Achard, J. Latham, R. Witt, and J. L. Weber. 2008. The most detailed portrait of Earth. European Space Agency 136:25–31.

Azzari, G., and D. B. Lobell. 2017. Landsat-based classification in the cloud: an opportunity for a paradigm shift in land cover monitoring. Remote Sensing of Environment 202:64–74.

Baig, M. H. A., L. Zhang, T. Shuai, and Q. Tong. 2014. Derivation of a tasseled cap transformation based on Landsat 8 at-satellite reflectance. Remote Sensing Letters 5:423–431.

Belgiu, M., and L. Drăguţ. 2016. Random forest in remote sensing: a review of applications and future directions. ISPRS Journal of Photogrammetry and Remote Sensing 114:24–31.

Booth, D. T., and P. T. Tueller. 2003. Rangeland monitoring using remote sensing. Arid Land Research and Management 17:455–467.

Breiman, L. 2001. Random Forests. Machine Learning 45:5–32.

Brooks, M. L., C. S. Brown, J. C. Chambers, C. M. D'Antonio, J. E. Keeley, and J. Belnap. 2016. Exotic annual Bromus invasions: Comparisons among species and ecoregions in the western United States. Pages 11–60 in M. J. Germino, J. C. Chambers, and C. S. Brown, editors. Exotic bromegrasses in arid and semiarid ecosystems of the western US. Springer International Publishing, Basel, Switzerland.

Bureau of Land Management (BLM). 2015. Soda fire post-fire emergency stabilization and burned area rehabilitation plan. Boise, Idaho, USA. https://eplanning.blm.gov/epl-front-office/projects/nepa/52963/63896/69241/J08B_SODA_ESR_Plan_9-30-15_electronicsig.pdf

Chambers, J. C., B. A. Bradley, C. S. Brown, C. D'Antonio, M. J. Germino, J. B. Grace, S. P. Hardegree, R. F. Miller, and D. A. Pyke. 2014. Resilience to stress and disturbance, and resistance to Bromus tectorum L. invasion in cold desert shrublands of western North America. Ecosystems 17:360–375.

Chambers, J. C., J. D. Maestas, D. A. Pyke, C. S. Boyd, M. Pellant, and A. Wuenschel. 2017. Using resilience and resistance concepts to manage persistent threats to sagebrush ecosystems and greater sage-grouse. Rangeland Ecology & Management 70: 149–164.

Chen, X., and H. Ishwaran. 2012. Random forests for genomic data analysis. Genomics 99:323–329.

Chen, J., et al. 2015. Global land cover mapping at 30 m resolution: a POK-based operational approach. ISPRS Journal of Photogrammetry and Remote Sensing 103:7–27.

Donchyts, G., F. Baart, H. Winsemius, N. Gorelick, J. Kwadijk, and N. van de Giesen. 2016. Earth's surface water change over the past 30 years. Nature Climate Change 6:810.

Friedl, M. A., D. Sulla-Menashe, B. Tan, A. Schneider, N. Ramankutty, A. Sibley, and X. Huang. 2010. MODIS Collection 5 global land cover: algorithm refinements and characterization of new datasets. Remote Sensing of Environment 114:168–182.

Genuer, R., J.-M. Poggi, and C. Tuleau-Malot. 2010. Variable selection using random forests. Pattern Recognition Letters 31:2225–2236.

Gómez, C., J. C. White, and M. A. Wulder. 2016. Optical remotely sensed time series data for land cover classification: a review. ISPRS Journal of Photogrammetry and Remote Sensing 116:55–72.

Gorelick, N., M. Hancher, M. Dixon, S. Ilyushchenko, D. Thau, and R. Moore. 2017. Google Earth Engine: planetary-scale geospatial analysis for everyone. Remote Sensing of Environment 202:18–27.

Hansen, M. C., et al. 2013. High-resolution global maps of 21st-century forest cover change. Science 342:850–853.

Havstad, K., et al. 2009. The Western United States Rangelands: A major resource. Pages 75–93 in W. F. Wedin and S. L. Fales, editors. Grassland quietness and strength for a new American Agriculture. ASA, CSSA, SSSA, Madison, Wisconsin, USA.

Herrick, J. E., J. W. Van Zee, S. E. McCord, E. M. Courtright, J. W. Karl, and L. M Burkett. 2017. Monitoring manual for grassland, shrubland, and savanna ecosystems. USDA-ARS Jornada Experimental Range, Las Cruces, New Mexico, USA.

Homer, C., J. Dewitz, L. Yang, S. Jin, P. Danielson, G. Xian, J. Coulston, N. Herold, J. Wickham, and K. Megown. 2015. Completion of the 2011 National Land Cover Database for the conterminous United States – Representing a decade of land cover change information. Photogrammetric Engineering and Remote Sensing 81:345–354.

Huang, J., H. Yu, A. Dai, Y. Wei, and L. Kang. 2017. Drylands face potential threat under 2°C global warming target. Nature Climate Change 7:417–422.

Hunt Jr., E. R., J. H. Everitt, J. C. Ritchie, M. S. Moran, D. T. Booth, G. L. Anderson, P. E. Clark, and M. S. Seyfried. 2003. Applications and research using remote sensing for rangeland management. Photogrammetric Engineering & Remote Sensing 69:675–693.

Lipsey, M. K., and D. E. Naugle. 2017. Precipitation and soil productivity explain effects of grazing on grassland songbirds. Rangeland Ecology & Management 70:331–340.

Louppe, G., L. Wehenkel, A. Sutera, and P. Geurts. 2013. Understanding variable importances in forests of randomized trees. Pages 431–439 in C. J. C. Burges, L. Bottou, M. Welling, Z. Ghahramani, and K. Q. Weinberger, editors. Advances in Neural Information Processing Systems 26. Curran Associates, Red Hook, New York, USA.

MacKinnon, W. C., J. W. Karl, G. R. Toevs, J. J. Taylor, S. Karl, C. S. Spurrier, and J. E. Herrick. 2011. BLM core terrestrial indicators and methods. U.S. Department of the Interior, Bureau of Land Management, National Operations Center, Denver, Colorado, USA.

Maestas, J. D., S. B. Campbell, J. C. Chambers, M. Pellant, and R. F. Miller. 2016. Tapping soil survey information for rapid assessment of sagebrush ecosystem resilience and resistance. Rangelands 38:120–128.

Marvin, D. C., L. P. Koh, A. J. Lynam, S. Wich, A. B. Davies, R. Krishnamurthy, E. Stokes, R. Starkey, and G. P. Asner. 2016. Integrating technologies for scalable ecology and conservation. Global Ecology and Conservation 7:262–275.

Masek, J. G., E. F. Vermote, N. E. Saleous, R. Wolfe, F. G. Hall, K. F. Huemmrich, F. Gao, J. Kutler, and T.-K. Lim. 2006. A Landsat surface reflectance dataset for North America, 1990–2000. IEEE Geoscience and Remote Sensing Letters 3:68–72.

McCord, S. E., M. Buenemann, J. W. Karl, D. M. Browning, and B. C. Hadley. 2017. Integrating remotely sensed imagery and existing multiscale field data to derive rangeland indicators: application of Bayesian additive regression trees. Rangeland Ecology & Management 70:644–655.

McCune, B., and D. Keon. 2002. Equations for potential annual direct incident radiation and heat load. Journal of Vegetation Science 13:603–606.

McIver, J. D., et al. 2010. SageSTEP: a regional experiment to evaluate effects of fire and fire surrogate treatments in the sagebrush biome. General Technical Report, RMRS-GTR-237, USDA Forest Service, Rocky Mountain Research Station, Ft. Collins, Colorado, USA.

Miller, R. F., J. C. Chambers, D. A. Pyke, F. B. Pierson, and C. J. Williams. 2013. A review of fire effects on vegetation and soils in the Great Basin region: response and ecological site characteristics (No. RMRS-GTR-308), USDA General Technical Report. U.S. Department of Agriculture, Forest Service, Rocky Mountain Research Station, Fort Collins, Colorado, USA.

Miller, R. F., S. T. Knick, D. A. Pyke, C. W. Meinke, S. E. Hanser, M. J. Wisdom, and A. L. Hild. 2011. Characteristics of sagebrush habitats and limitations to long-term conservation. Pages 145–185 in S. T. Knick and J. W. Connelly, editors. Greater sage-grouse—ecology and conservation of a landscape species and its habitats. Studies in Avian Biology 38. University of California Press, Berkeley, California, USA.

Miller, R. F., D. E. Naugle, J. D. Maestas, C. A. Hagen, and G. Hall. 2017. Woody invasion of western rangelands: using grouse as focal species for ecosystem restoration. Rangeland Ecology & Management 70:1–8.

Nobre, A. D., L. A. Cuartas, M. Hodnett, C. D. Rennó, G. Rodrigues, A. Silveira, M. Waterloo, and S. Saleska. 2011. Height above the nearest drainage—a hydrologically relevant new terrain model. Journal of Hydrology 404:13–29.

Ostfeld, R. S., S. T. A. Pickett, M. Shachak, and G. E. Likens. 1997. Defining the scientific issues. Pages 3–10 in S. T. A. Pickett, R. S. Ostfeld, M. Shachak, and G. E. Likens, editors. The ecological basis of conservation: Heterogeneity, ecosystems, and biodiversity. Springer US, Boston, Massachusetts, USA.

Pellant, M., P. Shaver, D. A. Pyke, and J. E. Herrick. 2005. Interpreting indicators of rangeland health, version 4. Technical Reference 1734-6. U.S. Department of the Interior, Bureau of Land Management, National Science and Technology Center, Denver, Colorado, USA. BLM/WO/ST-00/001 + 1734/REV05.

Pilliod, D. S., and J. L. Welty. 2013. Land treatment digital library: US Geological Survey Data Series 806. http://pubs.er.usgs.gov/publication/ds806

Pilliod, D. S., J. L. Welty, and R. S. Arkle. 2017a. Refining the cheatgrass-fire cycle in the Great Basin: precipitation timing and fine fuel composition predict wildfire trends. Ecology and Evolution 7:8126–8151.

Pilliod, D. S., J. L. Welty, and G. R. Toevs. 2017b. Seventy-five years of vegetation treatments on public rangelands in the Great Basin of North America. Rangelands 39:1–9.

R Core Team. 2017. R: A language and environment for statistical computing. R Foundation for Statistical Computing, Vienna, Austria.

Reeves, M. C., and J. E. Mitchell. 2011. Extent of coterminous US rangelands: quantifying implications of differing agency perspectives. Rangeland Ecology & Management 64:585–597.

Rennó, C. D., A. D. Nobre, L. A. Cuartas, J. V. Soares, M. G. Hodnett, J. Tomasella, and M. J. Waterloo. 2008. HAND, a new terrain descriptor using SRTM-DEM: mapping terra-firme rainforest environments in Amazonia. Remote Sensing of Environment 112:3469–3481.

Riley, K. L., I. C. Grenfell, and M. A. Finney. 2016. Mapping forest vegetation for the western United States using modified random forests imputation of FIA forest plots. Ecosphere 7:e01472.

Robinson, N. P., B. W. Allred, W. K. Smith, M. O. Jones, A. Moreno, T. A. Erickson, D. E. Naugle, and S. W. Running. 2018. Terrestrial primary production for the conterminous United States derived from Landsat 30 m and MODIS 250 m. Remote Sensing in Ecology and Conservation 33:121–138.

Running, S. W., and M. Zhao. 2015. Daily GPP and annual NPP (MOD17A2/A3) products NASA Earth Observing System MODIS land algorithm. MOD17 user's guide. https://lpdaac.usgs.gov/sites/default/files/public/product_documentation/mod17_user_guide.pdf

Ryan, K. C., and T. S. Opperman. 2013. LANDFIRE: a national vegetation/fuels data base for use in fuels treatment, restoration, and suppression planning. Forest Ecology and Management 294:208–216.

Sant, E. D., G. E. Simonds, R. D. Ramsey, and R. T. Larsen. 2014. Assessment of sagebrush cover using remote sensing at multiple spatial and temporal scales. Ecological Indicators 43:297–305.

Smith, J. T., J. S. Evans, B. H. Martin, S. Baruch-Mordo, J. M. Kiesecker, and D. E. Naugle. 2016. Reducing cultivation risk for at-risk species: predicting outcomes of conservation easements for sage-grouse. Biological Conservation 201:10–19.

Snaddon, J., G. Petrokofsky, P. Jepson, and K. J. Willis. 2013. Biodiversity technologies: tools as change agents. Biology Letters 9:20121029.

Soil Survey Staff. 2017. Gridded Soil Survey Geographic (gSSURGO) Database for the conterminous United States. United States Department of Agriculture, Natural Resources Conservation Service. http://datagateway.nrcs.usda.gov

USDA, NRCS. 2015. The National Resources Inventory grazing lands on-site database, 2004 – 2014 (Unreleased). Compiled by the Resource Inventory Division; processed by the Resource Assessment Division, Conservation Effects Assessment Project-Grazing Land Component.

USDA, NRCS. 2018. The PLANTS Database (http://plants.usda.gov). National Plant Data Team, Greensboro, North Carolina, USA.

USGS EROS. 2017. USGS product guide, Landsat surface reflectance-derived spectral indices version 3.5. https://landsat.usgs.gov/sites/default/files/documents/si_product_guide.pdf

Vermote, E., C. Justice, M. Claverie, and B. Franch. 2016. Preliminary analysis of the performance of the Landsat 8/OLI land surface reflectance product. Remote Sensing of Environment 185:46–56.

Wager, S., T. Hastie, and B. Efron. 2014. Confidence intervals for Random Forests: the jackknife and the infinitesimal jackknife. Journal of Machine Learning Research 15:1625–1651.

West, N. E. 2003. Theoretical underpinnings of rangeland monitoring. Arid Land Research and Management 17:333–346.

West, A. M., P. H. Evangelista, C. S. Jarnevich, S. Kumar, A. Swallow, M. W. Luizza, and S. M. Chignell. 2017. Using multi-date satellite imagery

to monitor invasive grass species distribution in post-wildfire landscapes: an iterative, adaptable approach that employs open-source data and software. International Journal of Applied Earth Observation and Geoinformation 59:135–146.

Wright, M., and A. Ziegler. 2017. ranger: a fast implementation of random forests for high dimensional data in C++ and R. Journal of Statistical Software 77:1–17.

Xian, G., C. Homer, D. Meyer, and B. Granneman. 2013. An approach for characterizing the distribution of shrubland ecosystem components as continuous fields as part of NLCD. ISPRS Journal of Photogrammetry and Remote Sensing 86:136–149.

Xian, G., C. Homer, M. Rigge, H. Shi, and D. Meyer. 2015. Characterization of shrubland ecosystem components as continuous fields in the northwest United States. Remote Sensing of Environment 168:286–300.

Supporting Information

Additional Supporting Information may be found online at: http://onlinelibrary.wiley.com/doi/10.1002/ecs2.2430/full